

1 On the statistical optimality of CO<sub>2</sub> atmospheric inversions assimilating CO<sub>2</sub>

2 column retrievals

3 Frédéric Chevallier<sup>1\*</sup>

4 21 September 2015

5

6 \* Corresponding author, E-mail: [frederic.chevallier@lsce.ipsl.fr](mailto:frederic.chevallier@lsce.ipsl.fr)

7 <sup>1</sup> Laboratoire des Sciences du Climat et de l'Environnement, CEA-CNRS-UVSQ, L'Orme des

8 Merisiers, Bat 701, 91191 Gif-sur-Yvette, France

9     **Abstract**

10    The extending archive of the Greenhouse Gases Observing SATellite (GOSAT) measurements  
11    (now covering about six years) allows increasingly robust statistics to be computed, that  
12    document the performance of the corresponding retrievals of the column-average dry air-mole  
13    fraction of CO<sub>2</sub> (XCO<sub>2</sub>). Here, we demonstrate that atmospheric inversions cannot be  
14    rigorously optimal when assimilating current XCO<sub>2</sub> retrievals, even with averaging kernels, in  
15    particular because retrievals and inversions use different assumption about prior uncertainty.  
16    We look for some practical evidence of this sub-optimality from the view point of atmospheric  
17    inversion by comparing a model simulation constrained by surface air-sample measurements  
18    with one of the GOSAT retrieval products (NASA's ACOS). The retrieval-minus-model  
19    differences result from various error sources, both in the retrievals and in the simulation: we  
20    discuss the plausibility of the origin of the major patterns. We find systematic retrieval errors  
21    over the dark surfaces of high-latitude lands and over African savannahs. More importantly,  
22    we also find a systematic over-fit of the GOSAT radiances by the retrievals over land for the  
23    high-gain detector mode, which is the usual observation mode. The over-fit is partially  
24    compensated by the retrieval bias-correction. These issues are likely common to other retrieval  
25    products and may explain some of the surprising and inconsistent CO<sub>2</sub> atmospheric inversion  
26    results obtained with the existing GOSAT retrieval products. We suggest that reducing the  
27    observation weight in the retrieval schemes (for instance so that retrieval increments to the  
28    retrieval prior values are halved for the studied retrieval product) would significantly improve  
29    the retrieval quality and reduce the need for (or at least reduce the complexity of) ad-hoc  
30    retrieval bias correction.

31

32

33      **1. Introduction**

34      CO<sub>2</sub> surface fluxes at the Earth's surface can be inferred from accurate surface measurements  
35      of CO<sub>2</sub> concentrations, but the sparseness of the current global network still leaves the flux  
36      horizontal and temporal gradients, and even their latitudinal distribution, very uncertain (Peylin et  
37      al. 2013). This limitation has provided a major incentive to develop the monitoring of CO<sub>2</sub>  
38      concentrations from space. First retrievals were obtained from existing instruments measuring  
39      either the thermal infrared radiation emitted by the atmosphere (Chédin et al. 2003) or the  
40      reflected sunlight in the near-infrared (NIR)/ shortwave infrared (SWIR) spectral regions  
41      (Buchwitz et al. 2005). The latter technique allows retrieving the column-average dry air-mole  
42      fraction of CO<sub>2</sub> (XCO<sub>2</sub>) while the former is not sensitive to CO<sub>2</sub> in the lower atmosphere, near  
43      the CO<sub>2</sub> sources and sinks. Since active (lidar) measurement techniques for XCO<sub>2</sub> from space are  
44      still in development (e.g., Ingmann et al. 2009), NIR/SWIR measurements currently offer the best  
45      prospect to provide “retrievals of CO<sub>2</sub> of sufficient quality to estimate regional sources and sinks”,  
46      as phrased by objective A.8.1 of the Global Climate Observing System programme (GCOS,  
47      2010), in the short term. However, they are hampered by uncertain knowledge about scatterers in  
48      the atmosphere at the corresponding wavelengths (aerosols and cirrus clouds) with an effect that  
49      varies with surface albedo, which is itself uncertain (e.g., Aben et al. 2007). Such interference in  
50      the XCO<sub>2</sub> signal seen in the NIR/SWIR measurements is of concern because even sub-ppm  
51      systematic errors (corresponding to less than 0.25% of the signal) can severely flaw the inversion  
52      of CO<sub>2</sub> surface fluxes (Chevallier et al. 2007, Miller et al. 2007). This risk motivated dedicated  
53      developments of the retrieval algorithms in order to de-convolve the spectral signatures of the  
54      involved compounds as much as possible (e.g., Reuter et al. 2010, Guerlet et al. 2013b).

55 The Japanese GOSAT, launched in January 2009, and the USA second Orbiting Carbon  
56 Observatory (OCO-2), launched in July 2014, observe the NIR/SWIR radiation with  
57 unprecedented spectral resolution in order to specifically address this remote sensing challenge.  
58 The GOSAT archive already covers six years and can provide good insight into the adequacy of  
59 NIR/SWIR retrievals for CO<sub>2</sub> source-sink inversion. In terms of random errors, raw GOSAT  
60 retrievals now reach single shot precision better than 2 ppm (one sigma) in fair measurement  
61 conditions (e.g., Nguyen et al. 2014). This performance is better than what pre-launch studies  
62 suggested: for instance Maksuytov et al. (2008) expected 2.5-10 ppm single shot precision only.  
63 Systematic errors are difficult to quantify or else they would be removed. They are likely state-  
64 dependent with absolute values varying in time and space about the ppm before any bias  
65 correction (Nguyen et al. 2014). They also depend on the retrieval algorithm (e.g., Oshchepkov et  
66 al. 2013). As expected, the remaining uncertainty has profound impact on CO<sub>2</sub> source-sink  
67 inversions (Basu et al. 2013, Chevallier et al. 2014), but XCO<sub>2</sub> retrievals have already served as  
68 a basis to study the carbon budgets of some regions (Guerlet et al. 2013a, Basu et al. 2014, Reuter  
69 et al. 2014). For instance, 25 scientists analysed several XCO<sub>2</sub> retrievals over continental Europe  
70 and concluded that the current understanding of the European carbon sink brought by bottom-up  
71 inventories had to be revisited (Reuter et al. 2014).

72 This paper aims at contributing to the debate about the relevance of current GOSAT retrievals  
73 for atmospheric inversions. Our starting point is a critical review of the basic principles behind  
74 the current processing chains that go in successive steps from GOSAT measured radiance spectra  
75 to surface flux estimates (Section 3). We then focus on the GOSAT retrievals provided by  
76 NASA's Atmospheric CO<sub>2</sub> Observations from Space project (ACOS, build 3.4, described in  
77 Section 2) for the period between June 2009 and May 2013. They are of particular interest  
78 because they have been processed in a way that prefigures the official OCO-2 retrievals in terms

79 of spectral bands and available simultaneous observations (O'Dell et al. 2012). In Section 4, we  
80 analyse the residuals between the ACOS-GOSAT retrievals and the simulated CO<sub>2</sub> concentration  
81 fields of the Monitoring Atmospheric Chemistry and Climate atmospheric inversion product  
82 (MACC, version 13r1, also described in Section 2) that assimilated surface air sample  
83 measurements from various networks. Concluding discussion follows in Section 5.

84

## 85 **2. Retrievals and model simulation**

86

### 87 **2.1. ACOS-GOSAT retrievals**

88

89 GOSAT is a joint venture by the Japan Aerospace Exploration Agency (JAXA), the National  
90 Institute for Environmental Studies (NIES) and the Ministry of the Environment (MOE) in Japan.  
91 This spacecraft is operated in a sun-synchronous polar orbit that crosses the Equator at about  
92 13:00 local time during daytime and that repeats every 3 days. As described by O'Dell et al.  
93 (2012) and Osterman et al. (2013), the ACOS algorithm retrieves XCO<sub>2</sub> from a selection of  
94 GOSAT measurements of reflected sunlight made in the same spectral bands than OCO-2. Over  
95 land, such measurements are made by pointing the instrument to the Earth on both sides of the  
96 satellite track. Given the low reflectivity of water surfaces, ocean measurements are only possible  
97 when the instrument is pointed to the sun-glint spot, which is only done within 40° from the  
98 Equator in the summer hemisphere. GOSAT also carries a cloud and aerosol imager that can help  
99 filtering difficult scenes out, but unlike other GOSAT retrieval algorithms, ACOS does not use it  
100 since OCO-2 does not contain a similar instrument.

101 Following Boesch et al. (2006) and Connor et al. (2008), the ACOS algorithm relies on  
102 optimal estimation (i.e. Bayesian methods) to retrieve the vertical profile of the CO<sub>2</sub> dry air mole

103 fraction together with variables interfering in the measurements: the surface pressure and the  
104 surface albedo, some variables describing temperature, water vapour, clouds and aerosols in the  
105 atmosphere, and channel offsets for the instrument. The retrieved  $\text{XCO}_2$  is simply obtained by  
106 integrating the retrieved  $\text{CO}_2$  profile. In this Bayesian formulation of the retrieval, prior  
107 information about  $\text{CO}_2$  is given an artificially small weight in order to maximize the observation  
108 contribution to the result: for instance, the standard deviation of the uncertainty assigned to the  
109 prior  $\text{XCO}_2$  is larger than 10 ppm (O'Dell et al., 2012), i.e. larger than typical variations of  $\text{XCO}_2$   
110 at the continental scale (e.g., Keppel-Aleks et al. 2011). We will discuss the impact of this choice  
111 later and for simplicity, we will call  $\text{XCO}_2^b$  and  $\text{XCO}_2^a$  the prior (*background*) and the retrieved  
112 (*analysed*)  $\text{XCO}_2$ , respectively.  $\text{XCO}_2^a$  can be compared with model simulations, as will be done  
113 here, or with other measurements via the associated  $\text{CO}_2$  averaging kernel profiles and prior  
114 profiles (e.g., Connor et al., 1994). For nadir viewing,  $\text{XCO}_2^a$  is representative of a volume that  
115 has a circular footprint at the Earth's surface of diameter about 10 km.

116 Previous comparisons between  $\text{XCO}_2^a$  and model simulations or reference ground-based  
117  $\text{XCO}_2$  measurements from Total Carbon Column Observing Network (TCCON) highlighted  
118 some systematic dependency of the error of  $\text{XCO}_2^a$  as a function of a series of internal variables  
119 of the algorithm (Wunch et al. 2011b). This feature reveals some limitations of the algorithm but  
120 also allows correcting them empirically, for instance before they are assimilated in atmospheric  
121 inversion systems (Crisp et al. 2012). We will call  $\text{XCO}_2^{a,c}$  the bias-corrected retrievals.

122

## 123 **2.2. MACC $\text{CO}_2$ inversion**

124

125 Since year 2011, the MACC pre-operational service ([www.copernicus-atmosphere.eu](http://www.copernicus-atmosphere.eu)) has  
126 been delivering a  $\text{CO}_2$  inversion product with biannual updates. Release 13r1 primarily describes

127 the CO<sub>2</sub> surface fluxes over more than three decades, from 1979 to 2013, at resolution 3.75° ×  
128 1.9° (longitude-latitude) and 3-hourly, based on 131 CO<sub>2</sub> dry air mole fraction station records  
129 (See Fig. S1) from three large databases:

130 • the NOAA Earth System Research Laboratory archive (NOAA CCGG,  
131 <http://www.esrl.noaa.gov/gmd/ccgg/index.html>),  
132 • the World Data Centre for Greenhouse Gases archive (WDCGG,  
133 <http://ds.data.jma.go.jp/gmd/wdcgg/>),  
134 • the Réseau Atmosphérique de Mesure des Composés à Effet de Serre database (RAMCES,  
135 <http://www.lsce.ipsl.fr/>).

136 The three databases include both in situ measurements made by automated quasi-continuous  
137 analysers and irregular air samples collected in flasks and later analyzed in central facilities. The  
138 detailed list of sites is provided in Tables S1 and S2.

139 The MACC Bayesian inversion method is formulated in a variational way in order to estimate  
140 the CO<sub>2</sub> surface fluxes at the above-described relatively high resolution over the globe  
141 (Chevallier et al. 2005, 2010). For v13r1, the system used a single 35-year inversion window,  
142 therefore enforcing physical and statistical consistency in the inverted fluxes. Fluxes and mole  
143 fractions are linked in the system by the global atmospheric transport model of the Laboratoire de  
144 Météorologie Dynamique (LMDZ, Hourdin et al. 2006) with 39 layers in the vertical and with the  
145 same horizontal resolution than the inverted fluxes. LMDZ is nudged to ECMWF-analysed winds  
146 for flux inversion.

147 The MACC inversion product also contains the 4D CO<sub>2</sub> field that is associated to the inverted  
148 surface fluxes through the LMDZ transport model. Simulating the GOSAT retrievals from this  
149 field is nearly straight-forward. The only difficulty lies in the interpolation from the LMDZ 39-  
150 level vertical grid to the 20-level vertical grid of the retrievals, before the retrieval averaging

151 kernels are applied. Indeed, the model orography at resolution  $3.75^\circ \times 1.9^\circ$  significantly differs  
152 from the high-resolution orography seen by the retrievals. For the interpolation, we assume that  
153  $\text{CO}_2$  concentrations vary linearly with the pressure in the vertical. When the model surface  
154 pressure is smaller than the retrieved surface pressure, the profile is artificially extended at  
155 constant value below the model surface. In the opposite case, model levels below the sounding  
156 surface are ignored. We compensate this artificial change of mass in the profile by systematically  
157 adjusting the interpolated profile so that its pressure-weighted mean equals that of the profile  
158 before the interpolation.

159

160 **3. Theoretical aspects**

161

162 Like the other retrieval and inversion systems (see, e.g., Oshchepkov et al., 2013, and Peylin et  
163 al., 2013), ACOS-GOSAT and MACC both follow the Bayesian paradigm in its Gaussian linear  
164 form (e.g., Rodgers, 2000) in order to estimate the most likely state, in a statistical sense, of the  
165  $\text{CO}_2$  profile and of the  $\text{CO}_2$  surface fluxes, respectively. In mathematical terms, given  $\mathbf{x}$  the vector  
166 that gathers the variables to be inferred (either a 1D  $\text{CO}_2$  profile or 2D+1D  $\text{CO}_2$  surface fluxes),  
167 given  $\mathbf{x}^b$  an a priori value of  $\mathbf{x}$  (coming from a climatology or from a model), and given  $\mathbf{y}$  the  
168 vector that gathers all relevant observations (either radiances or retrievals), the most likely state  
169 of  $\mathbf{x}$  is written:

170 
$$\mathbf{x}^a = \mathbf{x}^b + \mathbf{K}(\mathbf{y} - \mathbf{H} \mathbf{x}^b) \quad (1)$$

171  $\mathbf{H}$  is a linearized observation operator that links variables  $\mathbf{x}$  and  $\mathbf{y}$  (i.e. essentially a radiative  
172 transfer model or a transport model).  $\mathbf{K}$  is the following “Kalman gain” matrix:

173 
$$\mathbf{K} = \mathbf{B} \mathbf{H}^T (\mathbf{H} \mathbf{B} \mathbf{H}^T + \mathbf{R})^{-1} \quad (2)$$

174  $\mathbf{B}$  and  $\mathbf{R}$  are the error covariance matrices of  $\mathbf{x}^b$  and  $\mathbf{y}$ , respectively.

175 The error covariance matrix of  $\mathbf{x}^a$  is obtained by:

176 
$$\mathbf{A} = (\mathbf{I} - \mathbf{K}\mathbf{H}) \mathbf{B} \quad (3)$$

177 with  $\mathbf{I}$  the identity matrix with appropriate dimension.

178 For simplicity, Eq. (1) does not make other variables that are simultaneously inferred appear,  
179 like clouds, aerosols or surface variables for the retrievals, or the 3D state of CO<sub>2</sub> at the start of  
180 the assimilation window for the inversion.

181 The current processing chains that go from radiances to surface fluxes are two-step processes  
182 (let aside some attempts to introduce an additional intermediate step in the form of a short-  
183 window analysis of the 3D concentrations; Engelen et al. 2009). We now distinguish the retrieval  
184 process and the inversion process by putting breves  $\check{\cdot}$  on all symbols related to the former and  
185 hats  $\hat{\cdot}$  on all symbols related to the latter. In a first step, the CO<sub>2</sub> profiles and their uncertainty  
186  $\{\check{\mathbf{x}}^a, \check{\mathbf{A}}\}$  are retrieved for each sounding  $\{\check{\mathbf{y}}, \check{\mathbf{R}}\}$  separately. The resulting ensemble forms the  
187 observations to be simultaneously assimilated  $\{\hat{\mathbf{y}}, \hat{\mathbf{R}}\}$  for the second step. The presence of prior  
188 information  $\mathbf{x}^b$  in both steps complicates the transition between the two. Following Connor et al.  
189 (1994) and the current practice, we can technically eliminate the influence of  $\check{\mathbf{x}}^b$  (but not of its  
190 uncertainty) by the following adaptation of Eq. (1) in the second step: we assimilate  $\hat{\mathbf{y}}' = \check{\mathbf{x}}^a -$   
191  $(\mathbf{I} - \check{\mathbf{K}}\check{\mathbf{H}})\check{\mathbf{x}}^b = \check{\mathbf{K}}\check{\mathbf{y}}$  rather than  $\hat{\mathbf{y}}$  and change the observation operator from  $\hat{\mathbf{H}}$  to  $\hat{\mathbf{H}}' = \check{\mathbf{K}}\check{\mathbf{H}}\hat{\mathbf{H}}$ .  
192  $\check{\mathbf{K}}\check{\mathbf{H}}$  is called the retrieval *averaging kernel*. The retrieval error variances should consistently be  
193 reduced (e.g., Connor et al., 2008, paragraph 37) and is then called  $\hat{\mathbf{R}}'$  hereafter.

194 For simplicity, and without loss of generality in our linear framework, let us consider the  
195 assimilation of a single sounding  $\{\check{\mathbf{y}}, \check{\mathbf{R}}\}$  using its averaging kernel. By definition, given the  
196 changes made to  $\hat{\mathbf{H}}$  and  $\hat{\mathbf{R}}$ , the gain matrix changes as well and we call  $\hat{\mathbf{K}}'$  the new one. By

197 applying Eq. (1) in this configuration, the analysed surface fluxes can be directly expressed in a  
 198 concise form:

$$199 \quad \hat{\mathbf{x}}^a = \hat{\mathbf{x}}^b + \hat{\mathbf{K}}' \tilde{\mathbf{K}} (\tilde{\mathbf{y}} - \tilde{\mathbf{H}} \hat{\mathbf{H}} \hat{\mathbf{x}}^b) \quad (4)$$

200 This equation has the desired shape of Eq. (1), i.e. the sum of the prior value and of a linear  
 201 function of model-minus-measurement misfits. By construction, it does not depend on the  
 202 retrieval prior  $\tilde{\mathbf{x}}^b$ . However, to follow the optimal estimation framework, we still need to be able  
 203 to develop the product of the gain matrices consistently with Eq. (2), i.e. like (neglecting errors in  
 204 the observation operators):

$$205 \quad \mathbf{K} = \hat{\mathbf{B}} \hat{\mathbf{H}}^T \tilde{\mathbf{H}}^T (\tilde{\mathbf{H}} \hat{\mathbf{H}} \hat{\mathbf{B}} \hat{\mathbf{H}}^T \tilde{\mathbf{H}}^T + \tilde{\mathbf{R}})^{-1} \quad (5)$$

206 In practice, we see that:

$$207 \quad \hat{\mathbf{K}}' \tilde{\mathbf{K}} = \hat{\mathbf{B}} \hat{\mathbf{H}}'^T (\hat{\mathbf{H}}' \hat{\mathbf{B}} \hat{\mathbf{H}}'^T + \hat{\mathbf{R}}')^{-1} \tilde{\mathbf{B}} \tilde{\mathbf{H}}^T (\tilde{\mathbf{H}} \tilde{\mathbf{B}} \tilde{\mathbf{H}}^T + \tilde{\mathbf{R}})^{-1} \quad (6)$$

208 In the usual case when  $\tilde{\mathbf{H}} \neq \mathbf{I}$ , Eqs. (5-6) can be made consistent in general provided

$$209 \quad \tilde{\mathbf{H}} \tilde{\mathbf{B}} \tilde{\mathbf{H}}^T = \tilde{\mathbf{H}} \hat{\mathbf{H}} \hat{\mathbf{B}} \hat{\mathbf{H}}^T \tilde{\mathbf{H}}^T \quad (7)$$

210 and (by developing  $\hat{\mathbf{H}}'$  and using Eq. (7))

$$211 \quad \tilde{\mathbf{H}}^T \tilde{\mathbf{K}}^T (\tilde{\mathbf{K}} \tilde{\mathbf{H}} \tilde{\mathbf{B}} \tilde{\mathbf{H}}^T \tilde{\mathbf{K}}^T + \tilde{\mathbf{R}}')^{-1} \tilde{\mathbf{B}} = \mathbf{I} \quad (8)$$

212 Equation (7) simply expresses consistency between the prior error statistics within the  
 213 information content of the retrievals: the uncertainty of the retrieval prior and of the flux prior  
 214 should be the same in radiance space. This condition is not achieved by current satellite retrieval  
 215 algorithms, at least because they artificially maximize the measurement contribution in the  
 216 retrievals through the use of very large prior error variances (see Section 2.1 or Butz et al. 2009,  
 217 Reuter et al. 2010). However, if enough intermediate variables were saved by the retrieval  
 218 schemes, it would be possible to reconstruct the retrievals with appropriate prior error variances  
 219 and correlations.

220 Equation (8) can be satisfied in general if the retrieval averaging kernel  $\tilde{\mathbf{K}}\tilde{\mathbf{H}}$  is close to unity..  
221 In practice, the retrieval averaging kernel for profiles is far from unity because current radiance  
222 measurements do not provide any vertical resolution for CO<sub>2</sub>. The situation is better if the state  
223 vector  $\tilde{\mathbf{x}}$  is the integrated column (in that case  $\tilde{\mathbf{H}}$  includes an operator to distribute the column in  
224 the vertical).

225 As a consequence of deviations from Eqs (7-8), the effective gain matrix  $\tilde{\mathbf{K}}'\tilde{\mathbf{K}}$  significantly  
226 differs from the optimal one for GOSAT, resulting in a wrong balance between prior flux  
227 information and measured radiances. Overall,  $\tilde{\mathbf{K}}$  pulls too much towards the measured radiances  
228 and  $\tilde{\mathbf{K}}'$  pulls too much towards the prior. This suboptimality very likely flaws the 4D information  
229 flow from the radiance measurements to the surface flux estimates. In particular, the sub-  
230 optimality of  $\tilde{\mathbf{K}}$  affects the retrieval averaging kernel, that may not peak at the right height.

231 Migliorini (2012) proposed a sophisticated alternative to the averaging kernel assimilation of  
232 Connor et al. (1994), where the retrievals are assimilated after a linear transformation of both the  
233 retrievals and the observation operator. The transformation is heavier to implement than the  
234 above approach because it involves the retrieval signal-to-noise matrix  $\tilde{\mathbf{R}}^{-1/2}\tilde{\mathbf{H}}\tilde{\mathbf{B}}^{1/2}$ . It avoids  
235 the requirement of Eq. (8), but still requires consistent prior error statistics (Eq. (7)).

236 The situation complicates even further if we account for the facts that inversion systems  
237 assimilate bias-corrected retrievals (thereby implicitly re-introducing  $\tilde{\mathbf{x}}^b$  that had been neutralised  
238 by the use of averaging kernels, in the equations), that  $\tilde{\mathbf{H}}$  and  $\hat{\mathbf{H}}$  are imperfect operators, the  
239 uncertainty of which should be reported in  $\tilde{\mathbf{R}}$ , following Eq. (5), and that  $\tilde{\mathbf{H}}$  is usually non-linear.  
240 The need to report all observation operator uncertainties in  $\tilde{\mathbf{R}}$  means that retrieval configuration  
241 should in principle be tailored to the retrieval end-application, i.e. to the precision of the  
242 observation operator that is used in this end-application. For flux inversion, the transport model

243 uncertainty in  $\text{XCO}_2$  space is about 0.5 ppm (1  $\sigma$ , Houweling et al. 2010). When optimizing  
244 parameters of a flux model rather than for the flux themselves (in Carbon Cycle Data  
245 Assimilation Systems, Rayner et al. 2005), the uncertainty of the flux model equations has also to  
246 be reported in  $\tilde{\mathbf{R}}$ : when projected in the space of  $\text{XCO}_2$ , they are comparable to transport model  
247 uncertainties (Kuppel et al. 2013).

248

#### 249 **4. Practical aspects**

250

251 Given the particular concerns raised about the optimality of  $\text{XCO}_2$  retrievals and of their  
252 averaging kernels in the previous section, we now focus on one specific retrieval product, ACOS-  
253 GOSAT, in order to look for some practical evidence of this sub-optimality.

254

##### 255 **4.1. Mean differences**

256

257 Fig. 1 shows the mean bias-corrected retrievals  $\text{XCO}_2^{\text{a,c}}$  and the mean corresponding posterior  
258  $\text{XCO}_2$  field of the MACC inversion over the June 2009 – May 2013 period per  $3.75^\circ \times 1.9^\circ$  grid  
259 cell. All retrievals are used, provided they are found good by the ACOS standard quality control.  
260 The data density (Fig. 2b) follows the frequency of favourable retrieval conditions: more sunlight  
261 in the Tropics, less cloud over desert areas or over subsidence ocean regions. The long-term mean  
262 of the retrieval-minus-model differences (Fig. 2a) is usually about 1 ppm. Interestingly, it appears  
263 to be organized spatially. Over land, large positive values ( $> 0.5$  ppm, ACOS-GOSAT being  
264 larger) are seen over boreal forests, over most of South America, over grassland/cropland regions  
265 in Central Africa and over the West coast of the USA. Negative values occur over most of the  
266 other lands, with smaller values (up to  $\sim -1$  ppm) mostly over South and East Asia. Over the

267 oceans, values are mostly positive north of 30°N and south of 10°S, and negative in between.  
268 Both errors in ACOS-GOSAT and errors in the model simulations contribute to these differences,  
269 which complicates the interpretation of Fig. 2a. For instance, the zonal structure of the  
270 differences over the oceans could well be caused by the model, either because of too few surface  
271 air-sample sites in the Tropics or because the LMDZ transport model would not represent the  
272 inter-hemispheric exchange well enough (Patra et al. 2011). Alternatively, misrepresented clouds  
273 around the convergence zones could also induce them in the retrievals. Some of the patterns of  
274 Fig. 2a are similar to the surface cover, like the gradient between the Sahel and the African  
275 savannahs, or the one between the equatorial Atlantic and the African savannahs, while we  
276 expect the true XCO<sub>2</sub> fields to be first driven by large-scale horizontal advection (Keppel-Aleks  
277 et al. 2011). The main local spatial gradients in the mean differences are also seen on monthly  
278 means despite less data density (Fig. 3). They mostly reflect the retrieval gradients (Fig. 1a),  
279 because the model XCO<sub>2</sub> simulation is spatially smoother (Fig. 1b), even though it uses the  
280 retrieval averaging kernels (that change from scene to scene as a function, among other factors, of  
281 surface conditions) and even though it is sampled like the retrievals (i.e. with a spatially  
282 heterogeneous data density, also varying as a function, among other things, of surface conditions).

283 The jump of the long-term mean difference from the African savannahs to Sahel or equatorial  
284 Atlantic (while there is no jump between subtropical Atlantic and Western Sahara for instance)  
285 mostly corresponds to data from March (Fig. 3a), at the end of the savannah burning season (e.g.  
286 van der Werf et al. 2010). The model shows elevated values (Fig. 1b), but much less than the  
287 retrievals (Fig. 1a). If the model was underestimating the intensity of the fire, we would expect  
288 the mean difference to take the shape of a plume, i.e. to spread downstream the source region, but  
289 this is not the case. This suggests that the retrievals are affected by systematic errors over this  
290 region.

291 The positive differences of Fig. 2a in Eurasia notably follow the boreal forests, while negative  
292 values are found over the neighbouring regions of sparse tundra vegetation north of Siberia, or  
293 those of grassland/cropland south of them. The same remark applies to North America. The link  
294 with boreal forests is less obvious when looking at one isolated year because of the relatively  
295 small number of retrievals in these regions (not shown). The misfit pattern in Siberia and in North  
296 America contains many values larger than 1 ppm corresponding to relatively large retrieved  
297  $\text{XCO}_2$  (Fig. 1a). These large values are all the more surprising that retrievals in these high  
298 latitudes are obtained during the growing season and that boreal forests in Eurasia are identified  
299 as large carbon sinks by bottom-up inventories (Pan et al. 2011, Dolman et al. 2012). By  
300 comparison, we can look at agricultural regions, where the model could miss gradients during  
301 crop growth, both because the MACC inversion prior fluxes do not explicitly represent  
302 agricultural practices and because the location of the assimilated surface air-sample  
303 measurements only provides rough information about crop fluxes: the differences are marginal (-  
304 0.1 ppm on average, whether we compute the mean at the global scale or only for latitudes above  
305 40°N) for retrievals located in crop regions, as identified by the high-resolution land cover map of  
306 ESA's Land Cover Climate Change Initiative project (<http://www.esa-landcover-cci.org/>). In the  
307 Corn Belt, the intensively agricultural region in the Midwest of the USA, differences are negative,  
308 but they are much smaller in absolute value (the differences are larger than -0.4 ppm) than over  
309 the boreal forests, and the Corn Belt boundaries do not sharply appear, in particular on its eastern  
310 side. The Corn Belt does not particularly appear in monthly means either (e.g., Fig. 3b). These  
311 elements suggest that the long-term mean differences over boreal forests come from a retrieval  
312 artifact rather than from the MACC inversion product.

313 From a radiative transfer point of view, boreal forests are largely covered with needle-leaved  
314 trees with low albedo in the strong  $\text{CO}_2$  spectral band of GOSAT near 2.1  $\mu\text{m}$  (Fig. 4): these low

315 values hamper the  $\text{XCO}_2$  retrieval. O'Dell et al. (2012) already showed that large positive biases  
316 can occur for needle-leaved evergreen forests, with the retrieval exchanging surface albedo for  
317 very thin cloud or aerosol. Extreme cases are filtered out by the ACOS-GOSAT quality control,  
318 but Fig. 2a suggests that the remaining retrievals over boreal forests, including the region in  
319 Siberia East of 100°E which is dominated by deciduous needle-leaved trees with slightly larger  
320 albedos, are still biased. In temperate regions, south of 50°N, the differences for needle-leaf cover  
321 (mainly in Southeast USA and Southeast China) have the opposite sign, but they do not show up  
322 distinctly in the difference map like the boreal forests. Tropical forests in South America and in  
323 Africa also have low albedo and correspond to negative differences. They are more identifiable in  
324 Fig. 2a, but could be explained by an insufficient carbon sink in the model as well as by a  
325 retrieval artifact.

326

#### 327 **4.2. Link to the retrieval increment**

328

329 We now look at the  $\text{XCO}_2$  misfit statistics over land and for the high-gain mode as a function  
330 of the size of the retrieval increment to its prior information ( $\text{XCO}_2^a - \text{XCO}_2^b$ ) in Fig. 5. We look  
331 at the misfits of the model to  $\text{XCO}_2^a$ , to  $\text{XCO}_2^{a,c}$  and to  $\text{XCO}_2^b$ , in order to visualize the added  
332 value brought by the retrieval process and by the bias correction, successively, on top of the prior  
333 estimate. This prior estimate about atmospheric  $\text{CO}_2$  has been provided to the retrieval scheme by  
334 a data-driven empirical model (Wunch et al. 2011a). In Fig. 5, each bin along the abscissa  
335 encompasses a large diversity of times during the four years and a large diversity of locations  
336 over the globe, over which the model simulation should be overall more accurate (smaller root  
337 mean square error) than  $\text{XCO}_2^b$ ,  $\text{XCO}_2^a$  and even  $\text{XCO}_2^{a,c}$  (Chevallier and O'Dell 2013). Further,  
338 we expect the model error to be uncorrelated with the error of  $\text{XCO}_2^b$ ,  $\text{XCO}_2^a$  and  $\text{XCO}_2^{a,c}$  so that

339 a smaller standard deviation of the misfits (e.g., using  $\text{XCO}_2^a$  rather than  $\text{XCO}_2^b$ ) can be  
340 interpreted in terms of better precision of the corresponding retrieval quantity.

341 The mean difference significantly varies with the increment size: starting at 0.7 ppm for the  
342 smallest increments it reaches about 2 ppm and -1 ppm, for  $\text{XCO}_2^b$  and  $\text{XCO}_2^a$  respectively. As  
343 expected, the mean difference is systematically better with  $\text{XCO}_2^a$  than with  $\text{XCO}_2^b$ . The bias  
344 correction ( $\text{XCO}_2^{a,c}$ ) further reduces the mean difference to a small extent.

345 The standard deviation for  $\text{XCO}_2^b$  is 1.1 ppm for small increments and smoothly increases to 2  
346 ppm for retrieval increments of size 6 ppm. This trend demonstrates some skill of the retrieval  
347 algorithm to characterize the error of  $\text{XCO}_2^b$  from the GOSAT radiances and to generate a  
348 sizeable increment accordingly. By comparison, the model variability for a given increment size  
349 over the four years ranges between 3 and 4 ppm ( $1\sigma$ ), the prior variability is about 3 ppm and the  
350 retrieval variability ranges between 3 and 7 ppm. The standard deviation that uses  $\text{XCO}_2^a$  is 1.1  
351 ppm for small increments. It smoothly increases to 4 ppm for retrieval increments of size 6 ppm:  
352 it is systematically larger than the standard deviation that uses  $\text{XCO}_2^b$  (despite a smaller mean  
353 difference). The standard deviation that uses  $\text{XCO}_2^{a,c}$  is also 1.1 ppm for small increments and is  
354 also systematically larger than the standard deviation that uses  $\text{XCO}_2^b$ , but it performs better than  
355  $\text{XCO}_2^a$ . The worse standard deviation of the misfit of  $\text{XCO}_2^a$  and  $\text{XCO}_2^{a,c}$  to the model compared  
356 to  $\text{XCO}_2^b$  cannot be explained by a common lack of variability in the model and in  $\text{XCO}_2^b$  (that  
357 would correlate the model error with the that of  $\text{XCO}_2^b$ ), because (i) at the large scale, thinning  
358 the retrievals (for instance by keeping only one retrieval every nine model grid boxes for a given  
359 day) only marginally changes the figure (not shown), and (ii) at the sub-grid scale, the variability  
360 of  $\text{XCO}_2$  is usually well below the ppm (Alkhalef et al. 2008, Corbin et al. 2008), i.e. one order  
361 of magnitude smaller than the prior-to-retrieval degradation. Some, but not all, of the degradation  
362 is purely random and disappears after enough averaging (see Fig. 6 of Kulawik et al. 2015).

363 The fact that the standard deviation smoothly increases with increment size suggests that the  
364 increment size is systematically overestimated. Fig. 6 presents a simple test where we halve the  
365 retrieval increments, without any bias correction: we call  $XCO_2^{a,r} = XCO_2^b + (XCO_2^a - XCO_2^b)/2$   
366 the result. The reduction is seen to cancel most of the dependency of the statistics of the  
367 observation-minus-model misfits to the increment size: the standard deviation and the mean are  
368 then stable around 1.1 ppm and -0.3 ppm, respectively for increments up to 4 ppm without any  
369 bias correction. The standard deviation is systematically better than for  $XCO_2^b$ , which shows  
370 added value brought by the radiance measurements, in contrast to the previous results. This result  
371 also empirically confirms that the initial increments are in the right direction but are too large.

372 For the medium-gain retrievals (Fig. 7) and for the ocean glint retrievals (Fig. 8), the standard  
373 deviation of the misfits using  $XCO_2^{a,c}$  is not significantly larger than that using  $XCO_2^b$ .

374

## 375 **5. Discussion and conclusions**

376

377 Small uncertainties in aerosols, cirrus cloud or surface albedo are known to heavily affect the  
378 quality of the  $XCO_2$  satellite retrievals and to propagate into biases in the fluxes inverted from  
379 them, even when the parasite signal in  $XCO_2$  is sub-ppm. This weakness lead the science team of  
380 NASA's OCO, a satellite that failed at launch in February 2009, to conclude that the space-based  
381 NIR/SWIR measurements of  $XCO_2$  could not be used alone for  $CO_2$  source-sink inversions and  
382 that they had to be combined with observations from a reasonable number of surface stations  
383 (Miller et al. 2007). However, so much improvement has been obtained in these issues by various  
384 institutes during the last few years, that it is sometimes thought that the space-borne  $XCO_2$   
385 retrievals have reached sufficient quality for source-sink inversion. The present paper discusses

386 where we stand in this respect both from general theoretical considerations and from one of the  
387 most advanced GOSAT retrieval products.

388 From the theory, we have shown that a two-step approach to infer the surface fluxes from the  
389 GOSAT measured radiances, with CO<sub>2</sub> retrievals as an intermediate product, cannot be optimal.  
390 This suboptimality corrupts the 4D information flow from the radiance measurements to the  
391 surface flux estimates. It is amplified by the current retrieval strategy where prior errors are much  
392 larger (by an order of magnitude in terms of variances) than the performance of prior CO<sub>2</sub>  
393 simulations used in atmospheric inversions. Indeed, the use of averaging kernels makes  
394 atmospheric inversion insensitive to the choice of a particular retrieval prior CO<sub>2</sub> profile (Connor  
395 et al. 1994) if retrievals are assimilated without any bias correction, but it does not make the  
396 retrieval prior error statistics disappear from the inverse modelling equations. The current  
397 strategy likely generates retrieval averaging kernels that are inappropriate for atmospheric  
398 inversions in their default configurations, with a wrong vertical distribution and an excessive  
399 weight towards the measured radiances. Paradoxically, empirical bias correction of the retrievals  
400 (e.g., Wunch et al., 2011b) also contributes to the degradation of the 4D information flow,  
401 because it carries the imprint of the retrieval prior and of the retrieval prior error statistics. Direct  
402 assimilation of the measured radiances would solve the inconsistency, but would increase the  
403 computational burden of atmospheric inversions by several orders of magnitude. Alternatively,  
404 we could adapt the inversion systems to the current retrieval configuration by using minimal prior  
405 information about the surface fluxes, typically a flat prior flux field, but the result would still  
406 over-fit the measured radiances due to the absence of other (compensating) information.

407 We have compared the ACOS-GOSAT retrievals with a transport model simulation  
408 constrained by surface air-sample measurements in order to find some evidence of retrieval sub-  
409 optimality. Flaws in this transport model and in these inverted surface fluxes necessarily flaw the

410 simulation in many places over the globe and at various times of the year. We therefore carefully  
411 selected some of the relatively large discontinuities in the XCO<sub>2</sub> fields that the simulation  
412 unlikely generated. We found some evidence of retrieval systematic errors over the dark surfaces  
413 of the high-latitude lands and over African savannahs. We note that the mean differences over the  
414 African savannahs during the burning season could be explained by retrieval averaging kernels  
415 not peaking low enough in the atmosphere further to the assignment of inappropriate prior error  
416 correlations. Biomass burning aerosols that would not be well identified by the retrieval scheme  
417 could also play a role. We also found some evidence that the high-gain retrievals over land  
418 systematically over-fit the measured radiances, as a consequence of the prior uncertainty  
419 overestimation and of an underestimation of the observation uncertainty (as seen by the  
420 underlying radiative transfer model). This over-fit is partially compensated by the bias correction.  
421 An empirical test indicates that halving the retrieval increments without any posterior bias  
422 correction actually cancels the dependency of the statistics of the observation-minus-model  
423 misfits to the increment size and makes the standard deviation systematically better than for the  
424 retrieval prior XCO<sub>2</sub><sup>b</sup>, which shows added value brought by the radiance measurements, in  
425 contrast to the previous results. We argue here that the optimal-estimation retrieval process and,  
426 consequently, its posterior bias correction need retuning.

427 Given the diversity of existing satellite retrieval algorithms, our conclusions cannot be easily  
428 extrapolated to other GOSAT retrieval products and even less to XCO<sub>2</sub> retrievals from other  
429 instruments, but we note that such mistuning like the one highlighted here is common practice,  
430 both because the errors of the retrieval forward model are difficult to characterize and because  
431 satellite retrievals are usually explicitly designed to maximize the observation contribution, at the  
432 risk of over-fitting radiance and forward model noise. A primary consequence of this mistuning is  
433 the usual underestimation of retrieval errors: for instance, O'Dell et al. (2012) recommended

434 inflating this error by a twofold factor for ACOS-GOSAT b2.8. More importantly, our results  
435 show that the mistuning generates excessive (unphysical) space-time variations of the retrievals  
436 up to  $\sim 1\%$ . This noise level would not matter for short-lived species, but for CO<sub>2</sub> it is enough to  
437 significantly degrade the assimilation of the retrievals for flux inversion and may explain some of  
438 the inconsistency seen between GOSAT-based top-down results and bottom-up results for CO<sub>2</sub>  
439 (Chevallier et al. 2014, Reuter et al. 2014). Therefore, with the current mistuning, we reiterate  
440 previous recommendations to take GOSAT-based CO<sub>2</sub> inversion results particularly cautiously.  
441 But we also suggest that this situation may dramatically improve by simply retuning the retrieval  
442 schemes. Ultimately, internal statistical consistency of the retrievals and of the inversion schemes  
443 is needed to establish the credibility of their end product.

444

#### 445 **Acknowledgements**

446 Some of this work was performed using HPC resources of DSM-CCRT and of CCRT under  
447 the allocation t2014012201 made by GENCI (Grand Équipement National de Calcul Intensif). It  
448 was co-funded by the European Commission under the EU H2020 Programme (grant agreement  
449 No. 630080, MACC III). The ACOS GOSAT data can be obtained from <http://co2.jpl.nasa.gov>.  
450 They were produced by the ACOS/OCO-2 project at the Jet Propulsion Laboratory, California  
451 Institute of Technology, using GOSAT observed spectral radiances made available by the  
452 GOSAT project. The MACC product can be obtained from <http://www.copernicus-atmosphere.eu>.  
453 The author is very grateful to the many people involved in the surface CO<sub>2</sub> measurements and in  
454 the archiving of these data that were kindly made available to him. He thanks C. O'Dell for many  
455 fruitful and stimulating discussions about the topics addressed here. He also benefitted from  
456 interesting feedback from two anonymous reviewers and from Grégoire Broquet, Junjie Liu, Noel

457 Cressie, Sourish Basu, Kevin W. Bowman and Susan Kulawik in the discussion phase of the  
458 paper.

459

460 **References**

461 Aben, I., Hasekamp, O., and Hartmann, W.: Uncertainties in the space-based measurements of  
462 CO<sub>2</sub> columns due to scattering in the Earth's atmosphere, *J. Quant. Spectrosc. Radiat. Trans.*,  
463 104(3), 450–459, 2007

464 Alkhaled, A. A., Michalak, A. M., and Kawa, S. R.: Using CO<sub>2</sub> spatial variability to quantify  
465 representation errors of satellite CO<sub>2</sub> retrievals, *Geophys. Res. Lett.*, 35, L16813,  
466 doi:10.1029/2008GL034528, 2008.

467 Basu, S., Guerlet, S., Butz, A., Houweling, S., Hasekamp, O., Aben, I., Krummel, P., Steele, P.,  
468 Langenfelds, R., Torn, M., Biraud, S., Stephens, B., Andrews, A., and Worthy, D.: Global CO<sub>2</sub>  
469 fluxes estimated from GOSAT retrievals of total column CO<sub>2</sub>, *Atmos. Chem. Phys.*, 13, 8695–  
470 8717, doi:10.5194/acp-13-8695-2013, 2013.

471 Basu, S., M. Krol, A. Butz, C. Clerbaux, Y. Sawa, T. Machida, H. Matsueda, C. Frankenberg, O.  
472 P. Hasekamp, and I. Aben, The seasonal variation of the CO<sub>2</sub> flux over Tropical Asia estimated  
473 from GOSAT, CONTRAIL, and IASI, *Geophys. Res. Lett.*, 41, 1809–1815,  
474 doi:10.1002/2013GL059105, 2014.

475 Boesch, H., Toon, G. C., Sen, B., Washenfelder, R. A., Wennberg, P. O., Buchwitz, M., de Beek,  
476 R., Burrows, J. P., Crisp, D., Christi, M., Connor, B. J., Natraj, V., and Yung, Y. L.: Space-  
477 based near-infrared CO<sub>2</sub> measurements: Testing the Orbiting Carbon Observatory retrieval  
478 algorithm and validation concept using SCIAMACHY observations over Park Falls, Wisconsin,  
479 *J. Geophys. Res. Atmos.*, 111, D23302, doi:10.1029/2006JD007080, 2006.

480 Buchwitz, M., de Beek, R., Burrows, J. P., Bovensmann, H., Warneke, T., Notholt, J.,  
481 Meirink, J. F., Goede, A. P. H., Bergamaschi, P., Körner, S., Heimann, M., and Schulz, A.:  
482 Atmospheric methane and carbon dioxide from SCIAMACHY satellite data: initial comparison  
483 with chemistry and transport models, *Atmos. Chem. Phys.*, 5, 941-962, doi:10.5194/acp-5-941-  
484 2005, 2005.

485 Butz, A., Hasekamp, O. P., Frankenberg, C., and Aben, I.: Retrievals of atmospheric CO<sub>2</sub> from  
486 simulated space-borne measurements of backscattered near-infrared sunlight: accounting for  
487 aerosol effects, *Appl. Opt.*, 48, 3322–3336, doi:10.1364/AO.48.003322, 2009

488 Chédin, A., Serrar, S., Scott, N. A., Crevoisier, C., and Armante, R.: First global measurement of  
489 midtropospheric CO<sub>2</sub> from NOAA polar satellites: Tropical zone, *J. Geophys. Res.*, 108(D18),  
490 4581, doi:10.1029/2003JD003439, 2003..

491 Chevallier, F., Fisher, M., Peylin, P., Serrar, S., Bousquet, P., Bréon, F.-M., Chédin, A., and Ciais,  
492 P.: Inferring CO<sub>2</sub> sources and sinks from satellite observations: method and application to  
493 TOVS data, *J. Geophys. Res.*, 110, D24309, doi:10.1029/2005JD006390, 2005.

494 Chevallier, F.: Impact of correlated observation errors on inverted CO<sub>2</sub> surface fluxes from OCO  
495 measurements, *Geophys. Res. Lett.*, 34, L24804, doi:10.1029/2007GL030463, 2007.

496 Chevallier, F., Bréon, F.-M., and Rayner, P. J.: The contribution of the Orbiting Carbon  
497 Observatory to the estimation of CO<sub>2</sub> sources and sinks: Theoretical study in a variational data  
498 assimilation framework. *J. Geophys. Res.*, 112, D09307, doi:10.1029/2006JD007375, 2007.

499 Chevallier, F., Ciais, P., Conway, T. J., Aalto, T., Anderson, B. E., Bousquet, P., Brunke, E. G.,  
500 Ciattaglia, L., Esaki, Y., Fröhlich, M., Gomez, A., Gomez-Pelaez, A. J., Haszpra, L., Krummel,  
501 P. B., Langenfelds, R. L., Leuenberger, M., Machida, T., Maignan, F., Matsueda, H., Morgui, J.

502 A., Mukai, H., Nakazawa, T., Peylin, P., Ramonet, M., Rivier, L., Sawa, Y., Schmidt, M.,  
503 Steele, L. P., Vay, S. A., Vermeulen, A. T., Wofsy, S., and Worthy, D.: CO<sub>2</sub> surface fluxes at  
504 grid point scale estimated from a global 21-year reanalysis of atmospheric measurements. *J.*  
505 *Geophys. Res.*, 115, D21307, doi:10.1029/2010JD013887, 2010.

506

507 Chevallier, F., and O'Dell, C. W., Error statistics of Bayesian CO<sub>2</sub> flux inversion schemes as seen  
508 from GOSAT. *Geophys. Res. Lett.*, 40, 1252–1256, doi:10.1002/grl.50228, 2013.

509 Chevallier, F., Palmer, P. I., Feng, L., Boesch, H., O'Dell, C. W., and Bousquet, P.: Towards  
510 robust and consistent regional CO<sub>2</sub> flux estimates from in situ and space-borne measurements  
511 of atmospheric CO<sub>2</sub>, *Geophys. Res. Lett.*, 41, 1065–1070, doi:10.1002/2013GL058772, 2014.

512 Connor, B. J., Siskind, D. E., Tsou, J. J., Parrish, A., and Remsberg, E. E.: Ground-based  
513 microwave observations of ozone in the upper stratosphere and mesosphere, *J. Geophys. Res.*,  
514 99, 16,757–16,770, 1994.

515 Connor, B. J., Boesch, H., Toon, G., Sen, B., Miller, C., and Crisp, D.: Orbiting Carbon  
516 Observatory: Inverse method and prospective error analysis, *J. Geophys. Res. Atmos.*, 113,  
517 D05305, doi:10.1029/2006JD008336, 2008.

518 Corbin, K., Denning, A. S., Wang, J.-W., Lu, L., and Baker, I. T.: Possible representation errors  
519 in inversions of satellite CO<sub>2</sub> retrievals, *J. Geophys. Res.*, 113, D02301,  
520 doi:10.1029/2007JD008716, 2008.

521 Crisp, D., Fisher, B. M., O'Dell, C., Frankenberg, C., Basilio, R., Bösch, H., Brown, L. R.,  
522 Castano, R., Connor, B., Deutscher, N. M., Eldering, A., Griffith, D., Gunson, M., Kuze, A.,  
523 Mandrake, L., McDuffie, J., Messerschmidt, J., Miller, C. E., Morino, I., Natraj, V., Notholt, J.,

524 O'Brien, D. M., Oyafuso, F., Polonsky, I., Robinson, J., Salawitch, R., Sherlock, V., Smyth, M.,  
525 Suto, H., Taylor, T. E., Thompson, D. R., Wennberg, P. O., Wunch, D., and Yung, Y. L.: The  
526 ACOS CO<sub>2</sub> retrieval algorithm – Part II: Global XCO<sub>2</sub> data characterization,  
527 Atmos. Meas. Tech., 5, 687–707, doi:10.5194/amt-5-687-2012, 2012.

528 Dolman, A. J., Shvidenko, A., Schepaschenko, D., Ciais, P., Tchekabakova, N., Chen, T.,  
529 van der Molen, M. K., Belelli Marchesini, L., Maximov, T. C., Maksyutov, S., and Schulze, E.-  
530 D.: An estimate of the terrestrial carbon budget of Russia using inventory-based, eddy  
531 covariance and inversion methods, Biogeosciences, 9, 5323-5340, doi:10.5194/bg-9-5323-2012,  
532 2012.

533 Engelen, R. J., Serrar, S., and Chevallier, F.: Four-dimensional data assimilation of atmospheric  
534 CO<sub>2</sub> using AIRS observations, J. Geophys. Res., 114, D03303, doi:10.1029/2008JD010739,  
535 2009.

536 Global Climate Observing System (GCOS), Systematic observation requirements for satellite-  
537 based products for climate, Supplemental details to the satellite-based component of the  
538 “Implementation Plan for the Global Observing System for Climate in Support of the UNFCCC  
539 (2010 update)”, Prepared by World Meteorological Organization (WMO), Intergovernmental  
540 Oceanographic Commission, United Nations Environment Programme (UNEP), International  
541 Council for Science, Doc.: GCOS 154, 2010.

542 Guerlet, S., S. Basu, A. Butz, M. C. Krol, P. Hahne, S. Houweling, O. P. Hasekamp, and I. Aben,  
543 Reduced carbon uptake during the 2010 Northern Hemisphere summer as observed from  
544 GOSAT, Geophys. Res. Lett., 40, 2378–2383, doi:10.1002/grl.50402, 2013a.

545 Guerlet, S., Butz, A., Schepers, D., Basu, S., Hasekamp, O. P., Kuze, A., Yokota, T., Blavier, J.-  
546 F., Deutscher, N. M., Griffith, D. W. T., Hase, F., Kyrö, E., Morino, I., Sherlock, V., Sussmann,

547 R., Galli, A., and Aben, I.: Impact of aerosol and thin cirrus on retrieving and validating XCO<sub>2</sub>  
548 from GOSAT shortwave infrared measurements, *J. Geophys. Res. Atmos.*, 118, 4887–4905,  
549 doi:10.1002/jgrd.50332, 2013b.

550 Hourdin, F., Musat, I., Bony, S., Braconnot, P., Codron, F., Dufresne, J. L., Fairhead, L., Filiberti,  
551 M. A., Friedlingstein, P., Grandpeix, J. Y., Krinner, G., Levan, P., Li, Z. X., and Lott, F.: The  
552 LMDZ4 general circulation model: climate performance and sensitivity to parametrized physics  
553 with emphasis on tropical convection, *Climate Dynamics*, 27, 787-813, doi:10.1007/s00382-  
554 006-0158-0, 2006.

555 Houweling, S., Aben, I., Breon, F.-M., Chevallier, F., Deutscher, N., Engelen, R., Gerbig, C.,  
556 Griffith, D., Hungershoefer, K., Macatangay, R., Marshall, J., Notholt, J., Peters, W., and  
557 Serrar, S.: The importance of transport model uncertainties for the estimation of CO<sub>2</sub> sources  
558 and sinks using satellite measurements, *Atmos. Chem. Phys.*, 10, 9981-9992, doi:10.5194/acp-  
559 10-9981-2010, 2010.

560 Ingmann, P.: A-SCOPE, Advanced Space Carbon and Climate Observation of Planet Earth,  
561 Report of Assessment, SP-1313/1, ESA Communication Product Office, Noordwijk, The  
562 Netherlands, 2009.

563 Keppel-Aleks, G., Wennberg, P. O., and Schneider, T.: Sources of variations in total column  
564 carbon dioxide, *Atmos. Chem. Phys.*, 11, 3581–3593, doi:10.5194/acp-11-3581-2011, 2011.

565 Kulawik, S. S., Wunch, D., O'Dell, C., Frankenberg, C., Reuter, M., Oda, T., Chevallier, F.,  
566 Sherlock, V., Buchwitz, M., Osterman, G., Miller, C., Wennberg, P., Griffith, D. W. T.,  
567 Morino, I., Dubey, M., Deutscher, N. M., Notholt, J., Hase, F., Warneke, T., Sussmann, R.,  
568 Robinson, J., Strong, K., Schneider, M., and Wolf, J.: Consistent evaluation of GOSAT,

569 SCIAMACHY, CarbonTracker, and MACC through comparisons to TCCON, *Atmos. Meas.*  
570 *Tech. Discuss.*, 8, 6217-6277, doi:10.5194/amt-8-6217-2015, 2015.

571 Kuppel, S., Chevallier, F. and Peylin, P.: Quantifying the model structural error in Carbon Cycle  
572 Data Assimilation Systems. *Geosci. Model Dev.*, 6, 45-55, [doi:10.5194/gmd-6-45-2013](https://doi.org/10.5194/gmd-6-45-2013), 2013.

573 Maksyutov, S., Kadygrov, N., Nakatsuka, Y., Patra, P. K., Nakazawa, T., Yokota, T. and Inoue,  
574 G.: Projected impact of the GOSAT observations on regional CO<sub>2</sub> flux estimations as a function  
575 of total retrieval error, *J. Remote Sens. Soc. Jpn.*, 28, 190–197, 2008.

576 Migliorini, S.: On the equivalence between radiance and retrieval assimilation. *Mon. Wea. Rev.*,  
577 140, 258-265. doi:10.1175/MWR-D-10-05047.1, 2012.

578 Miller, C. E., Crisp, D., DeCola, P. L., Olsen, S. C., Randerson, J. T., Michalak, A. M., Alkhaled,  
579 A., Rayner, P., Jacob, D. J., Suntharalingam, P., Jones, D. B. A., Denning, A. S., Nicholls, M.  
580 E., Doney, S. C., Pawson, S., Boesch, H., Connor, B. J., Fung, I. Y., O'Brien, D., Salawitch, R.  
581 J., Sander, S. P., Sen, B., Tans, P., Toon, G. C., Wennberg, P. O., Wofsy, S. C., Yung, Y. L.,  
582 and Law, R. M.: Precision requirements for space-based XCO<sub>2</sub> data, *J. Geophys. Res.*, 112,  
583 D10314, doi:10.1029/2006JD007659, 2007.

584 Nguyen, H., Osterman, G., Wunch, D., O'Dell, C., Mandrake, L., Wennberg, P., Fisher, B., and  
585 Castano, R.: A method for colocating satellite XCO<sub>2</sub> data to ground-based data and its  
586 application to ACOS-GOSAT and TCCON, *Atmos. Meas. Tech.*, 7, 2631-2644,  
587 doi:10.5194/amt-7-2631-2014, 2014.

588 O'Dell, C. W., Connor, B., Bösch, H., O'Brien, D., Frankenberg, C., Castano, R., Christi, M.,  
589 Eldering, D., Fisher, B., Gunson, M., McDuffie, J., Miller, C. E., Natraj, V., Oyafuso, F.,  
590 Polonsky, I., Smyth, M., Taylor, T., Toon, G. C., Wennberg, P. O., and Wunch, D.: The ACOS  
591 CO<sub>2</sub> retrieval algorithm – Part 1: Description and validation against synthetic observations,  
592 *Atmos. Meas. Tech.*, 5, 99–121, doi:10.5194/amt-5-99-2012, 2012.

593 Oshchepkov, S., Bril, A., Yokota, T., Wennberg, P. O., Deutscher, N. M., Wunch, D., Toon, G.  
594 C., Yoshida, Y., O'Dell, C. W., Crisp, D., Miller, C. E., Frankenberg, C., Butz, A., Aben, I.,  
595 Guerlet, S., Hasekamp, O., Boesch, H., Cogan, A., Parker, R., Griffith, D., Macatangay, R.,  
596 Notholt, J., Sussmann, R., Rettinger, M., Sherlock, V., Robinson, J., Kyrö, E., Heikkinen, P.,  
597 Feist, D. G., Morino, I., Kadygrov, N., Belikov, D., Maksyutov, S., Matsunaga, T., Uchino, O.,  
598 and Watanabe, H.: Effects of atmospheric light scattering on spectroscopic observations of  
599 greenhouse gases from space. Part 2: Algorithm intercomparison in the GOSAT data processing  
600 for CO<sub>2</sub> retrievals over TCCON sites, J. Geophys. Res., 118, 1493-1512,  
601 doi:10.1002/jgrd.50146, 2013.  
602 Osterman, G., Eldering, A., Avis, C., O'Dell, C., Martinez, E., Crisp, D., Frankenberg, C., and  
603 Frankenberg, B., ACOS Level 2 Standard Product Data User's Guide v3.4, Revision Date:  
604 Revision B, 3 October 2013, available at:  
605 [https://co2.jpl.nasa.gov/static/docs/v3.4\\_DataUsersGuide-RevB\\_131028.pdf](https://co2.jpl.nasa.gov/static/docs/v3.4_DataUsersGuide-RevB_131028.pdf) (last access: 20  
606 April 2015), 2013.  
607 Pan, Y., Birdsey, R. A., Fang, J., Houghton, R., Kauppi, P. E., Kurz, W. A., Phillips, O. L.,  
608 Shvidenko, A., Lewis, S. L., Canadell, J. G., Ciais, P., Jackson, J. B., Pacala, S., McGuire, A.  
609 D., Piao, S., Rautiainen, A., Sitch, S., and Hayes, D.: A large and persistent carbon sink in the  
610 world's forests, Science, 333, 988–993, 2011.  
611 Patra, P. K., Houweling, S., Krol, M., Bousquet, P., Belikov, D., Bergmann, D., Bian, H.,  
612 Cameron-Smith, P., Chipperfield, M. P., Corbin, K., Fortems-Cheiney, A., Fraser, A., Gloor, E.,  
613 Hess, P., Ito, A., Kawa, S. R., Law, R. M., Loh, Z., Maksyutov, S., Meng, L., Palmer, P. I.,  
614 Prinn, R. G., Rigby, M., Saito, R., and Wilson, C.: TransCom model simulations of CH<sub>4</sub> and  
615 related species: linking transport, surface flux and chemical loss with CH<sub>4</sub> variability in the

616 troposphere and lower stratosphere, *Atmos. Chem. Phys.*, 11, 12813-12837, doi:10.5194/acp-  
617 11-12813-2011, 2011..

618 Peng, S., Ciais, P., Chevallier, F., Peylin, P., Cadule, P., Sitch, S., Piao, S., Ahlström, A.,  
619 Huntingford, C., Levy, P., Li, X., Liu, Y., Lomas, M., Poulter, B., Viovy, N., Wang, T., Wang,  
620 X., Zaehle, S., Zeng, N., Zhao, F., and Zhao, H.:Benchmarking the seasonal cycle of CO<sub>2</sub>  
621 fluxes simulated by terrestrial ecosystem models, *Global Biogeochem. Cycles*, 29, 46–64,  
622 doi:10.1002/2014GB004931, 2015.

623 Peylin, P., Law, R. M., Gurney, K. R., Chevallier, F., Jacobson, A. R., Maki, T., Niwa, Y.,  
624 Patra, P. K., Peters, W., Rayner, P. J., Rödenbeck, C., van der Laan-Luijkx, I. T., and  
625 Zhang, X.: Global atmospheric carbon budget: results from an ensemble of atmospheric CO<sub>2</sub>  
626 inversions, *Biogeosciences*, 10, 6699-6720, doi:10.5194/bg-10-6699-2013, 2013.

627 Rayner, P., Scholze, M., Knorr, W., Kaminski, T., Giering, R., and Widmann, H.: Two decades  
628 of terrestrial Carbon fluxes from a Carbon Cycle Data Assimilation System (CCDAS), *Global*  
629 *Biogeochem. Cy.*, 19, GB2026, doi:10.1029/2004GB002254, 2005

630 Reuter, M., Buchwitz, M., Schneising, O., Heymann, J., Bovensmann, H., and Burrows, J. P.: A  
631 method for improved SCIAMACHY CO<sub>2</sub> retrieval in the presence of optically thin clouds,  
632 *Atmos. Meas. Tech.*, 3, 209-232, doi:10.5194/amt-3-209-2010, 2010.

633 Reuter, M., Buchwitz, M., Hilker, M., Heymann, J., Schneising, O., Pillai, D., Bovensmann, H.,  
634 Burrows, J. P., Bösch, H., Parker, R., Butz, A., Hasekamp, O., O'Dell, C. W., Yoshida, Y.,  
635 Gerbig, C., Nehrkorn, T., Deutscher, N. M., Warneke, T., Notholt, J., Hase, F., Kivi, R.,  
636 Sussmann, R., Machida, T., Matsueda, H., and Sawa, Y.: Satellite-inferred European carbon  
637 sink larger than expected, *Atmos. Chem. Phys.*, 14, 13739–13753, doi:10.5194/acp-14-13739-  
638 2014, 2014.

639 Rodgers, C.D.: Inverse Methods for Atmospheric Sounding: Theory and Practice, World  
640 Scientific Publishing Co. Ltd., London, 2000.

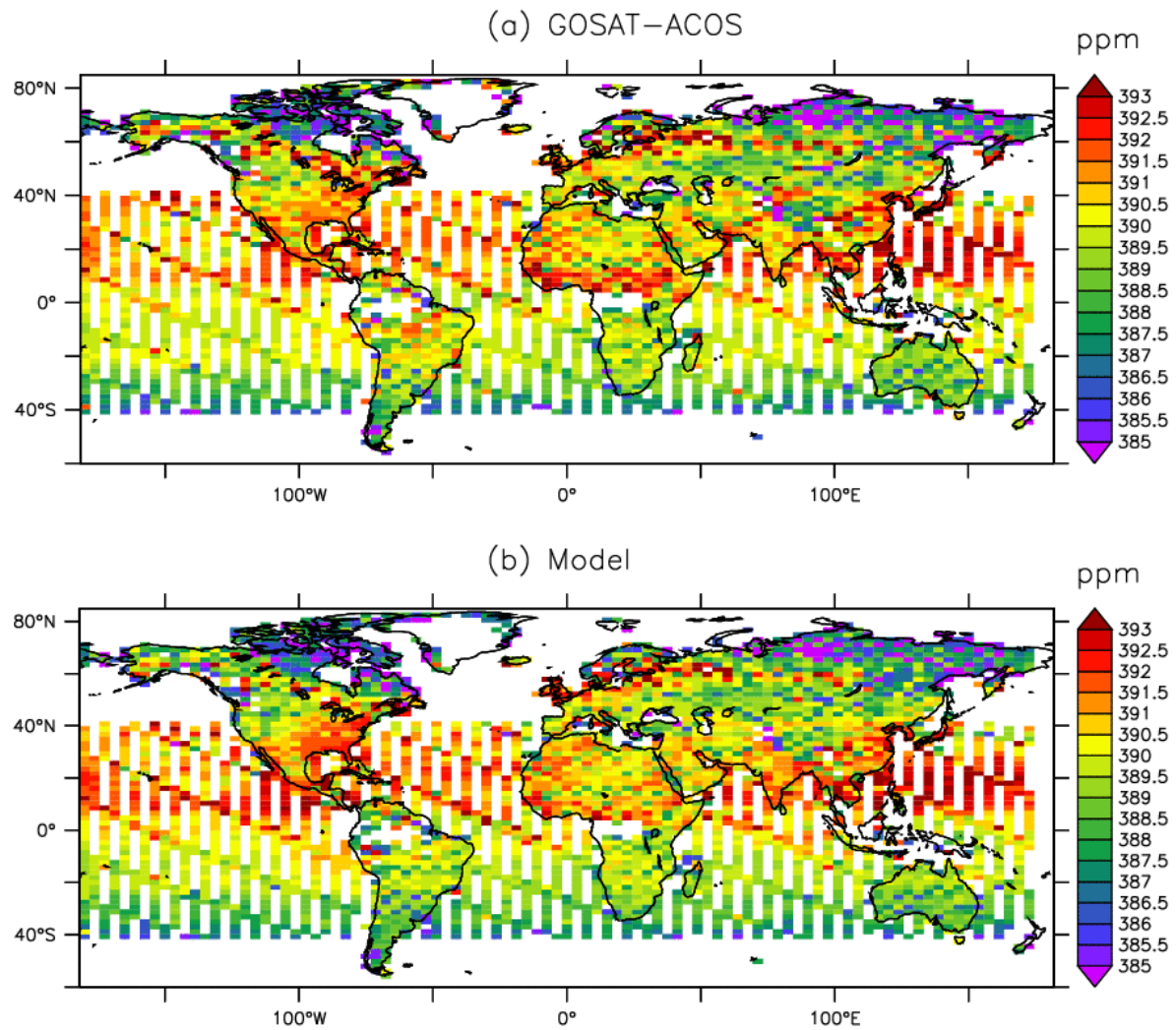
641 van der Werf, G. R., Randerson, J. T., Giglio, L., Collatz, G. J., Mu, M., Kasibhatla, P. S.,  
642 Morton, D. C., DeFries, R. S., Jin, Y., and van Leeuwen, T. T.: Global fire emissions and the  
643 contribution of deforestation, savanna, forest, agricultural, and peat fires (1997–2009), Atmos.  
644 Chem. Phys., 10, 11,707–11,735, doi:10.5194/acp-10-11707-2010, 2010.

645 Wunch, D., Toon, G. C., Blavier, J.-F. L., Washenfelder, R. A., Notholt, J., Connor, B. J., Griffith,  
646 D. W. T., Sherlock, V., and Wennberg, P. O., The Total Carbon Column Observing Network,  
647 Phil. Trans. R. Soc. A:2011369 2087-2112;DOI: 10.1098/rsta.2010.0240, 2011a.

648 Wunch, D., Wennberg, P. O., Toon, G. C., Connor, B. J., Fisher, B., Osterman, G. B.,  
649 Frankenberg, C., Mandrake, L., O'Dell, C., Ahonen, P., Biraud, S. C., Castano, R., Cressie, N.,  
650 Crisp, D., Deutscher, N. M., Eldering, A., Fisher, M. L., Griffith, D. W. T., Gunson, M.,  
651 Heikkinen, P., Keppel-Aleks, G., Kyrö, E., Lindenmaier, R., Macatangay, R., Mendonca, J.,  
652 Messerschmidt, J., Miller, C. E., Morino, I., Notholt, J., Oyafuso, F. A., Rettinger, M.,  
653 Robinson, J., Roehl, C. M., Salawitch, R. J., Sherlock, V., Strong, K., Sussmann, R., Tanaka, T.,  
654 Thompson, D. R., Uchino, O., Warneke, T., and Wofsy, S. C.: A method for evaluating bias in  
655 global measurements of CO<sub>2</sub> total columns from space, Atmos. Chem. Phys., 11, 12317–12337,  
656 doi:10.5194/acp-11-12317-2011, 2011b.

657

658



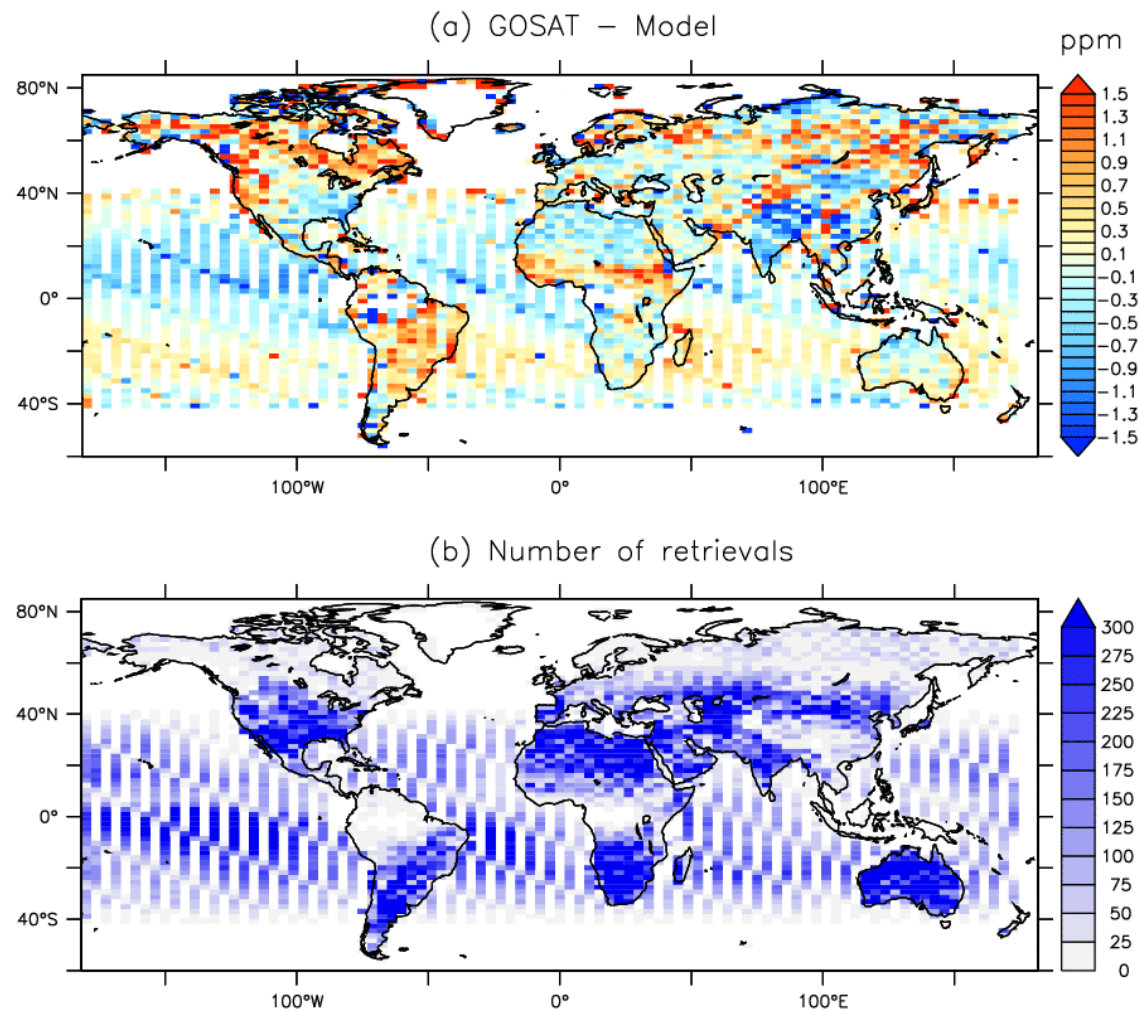
659

660 **Fig. 1. (a) Mean ACOS-GOSAT bias-corrected retrievals in the model grid over 4 years**

661 **(June 2009-May 2013). (b) Corresponding mean CO<sub>2</sub> 4D field associated to the MACC CO<sub>2</sub>**

662 **inversion (computed using the averaging kernels and the prior profiles of the retrievals).**

663



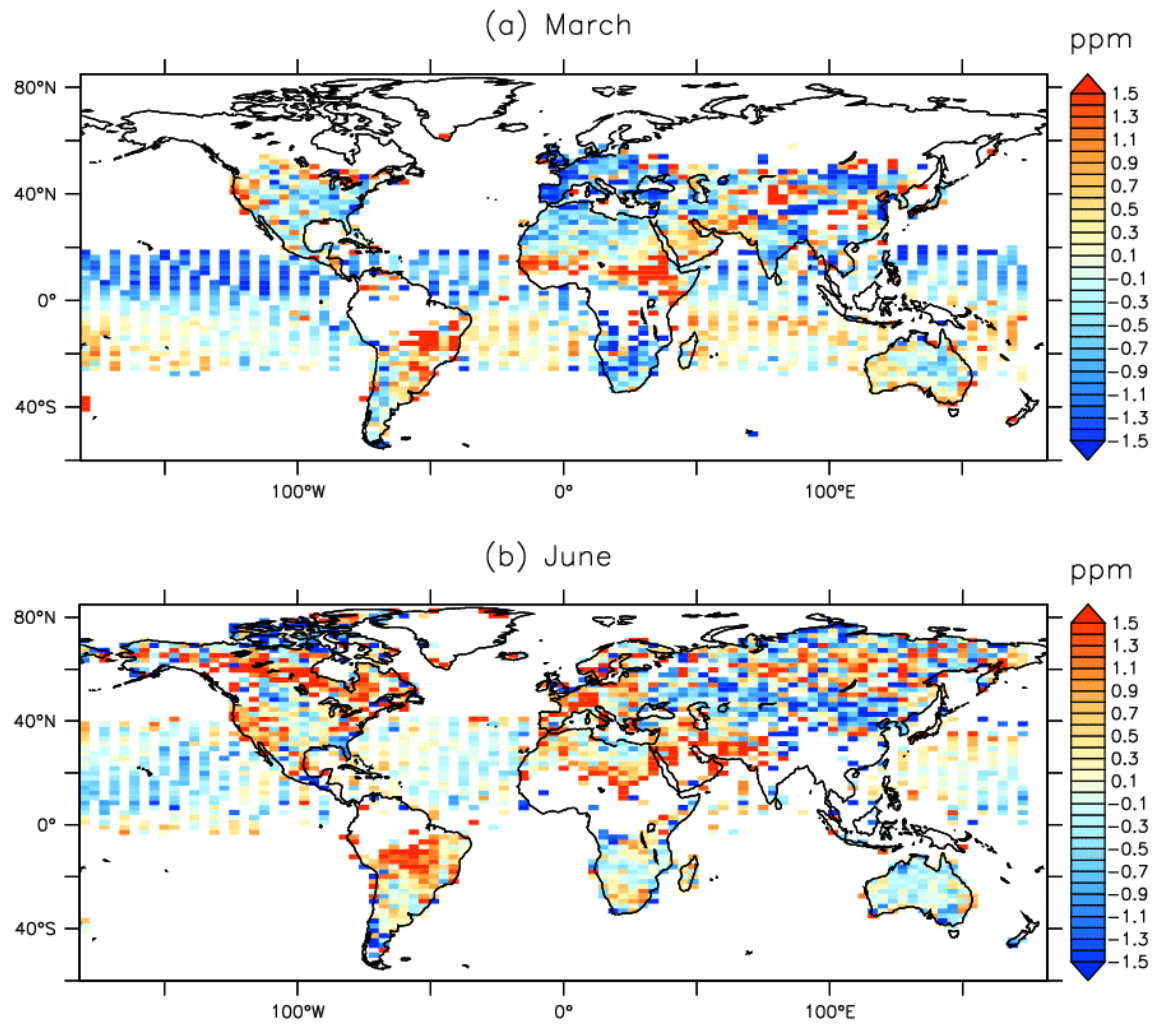
664

665

666 **Fig. 2. (a) Mean difference between the maps of Fig. 1 (retrievals minus model). (b)**

667 **Corresponding number of retrievals.**

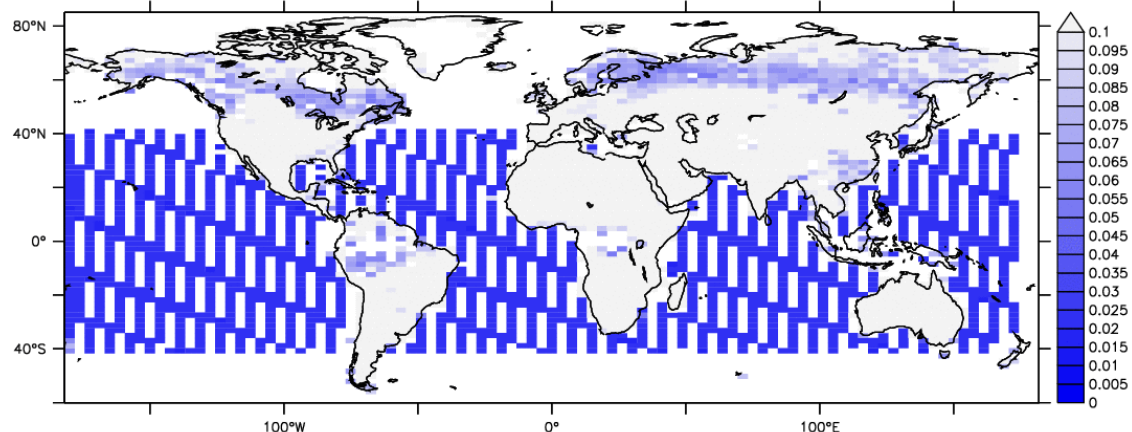
668



669  
670  
671  
672

**Fig. 3. Same as Fig. 2(a) (retrievals minus model), but focussing on the months of March and June.**

673

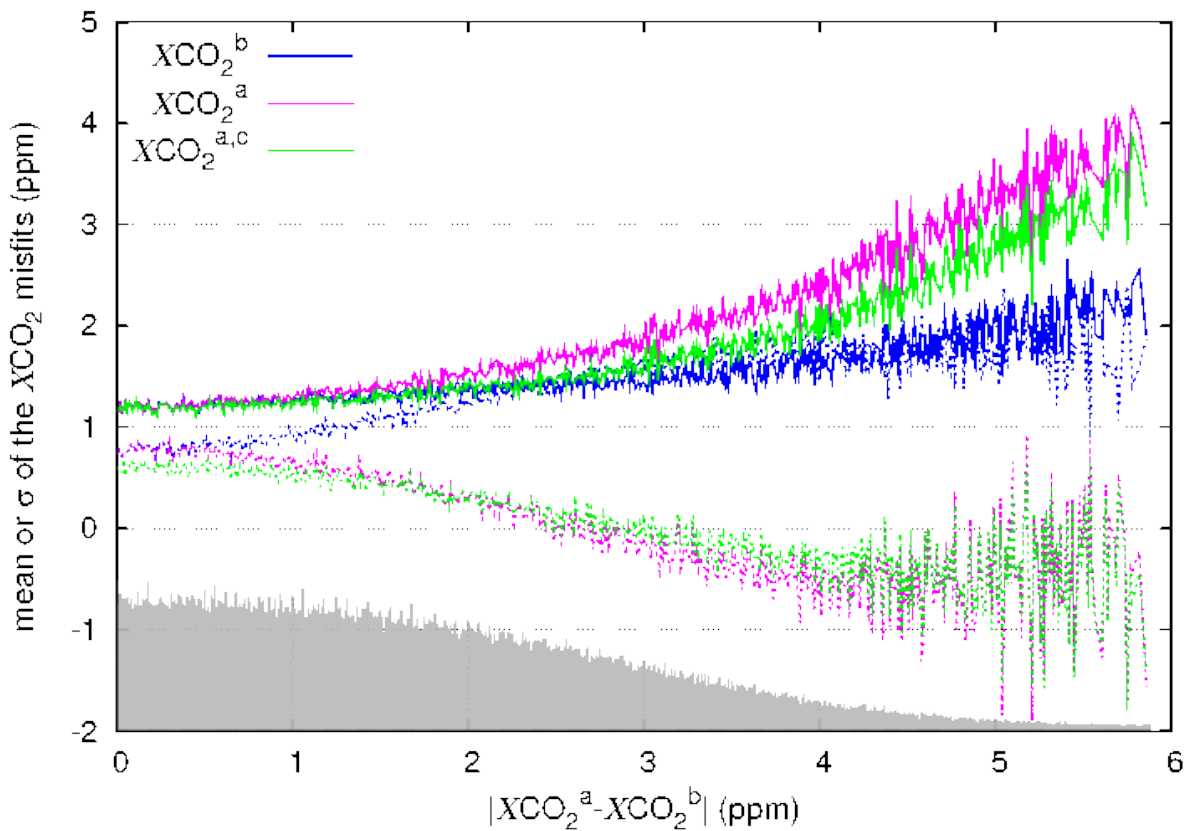


674

675 **Fig. 4. Mean surface albedo retrieved in the strong CO<sub>2</sub> band by ACOS-GOSAT in the**  
676 **model grid over 4 years (June 2009-May 2013). The blue scale focuses on the values less**  
677 **than 0.1.**

678

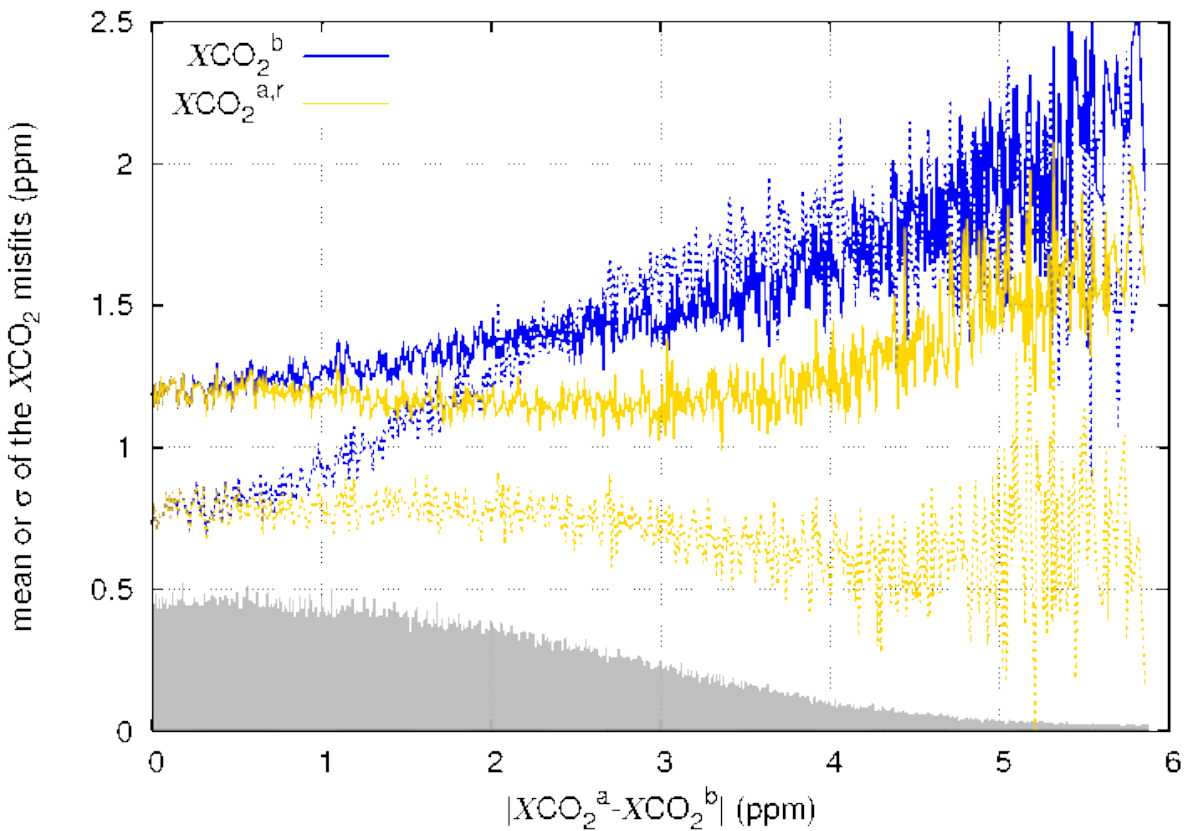
679



680

681 **Fig. 5. Mean and standard deviation of the retrieval-minus-model misfits between June**  
 682 **2009 and May 2013 for the high-gain mode retrievals over land as a function of the retrieval**  
 683 **increment size. The statistics are also shown for the prior-minus-model misfit. The model**  
 684 **values are raw pressure-weighted columns and do not account for the averaging kernels in**  
 685 **order not to correlate the two axes (in practice, using the averaging kernels actually does**  
 686 **not significantly affect the standard deviations shown). The grey shade shows the**  
 687 **distribution of the retrieval density (axis not shown).**

688

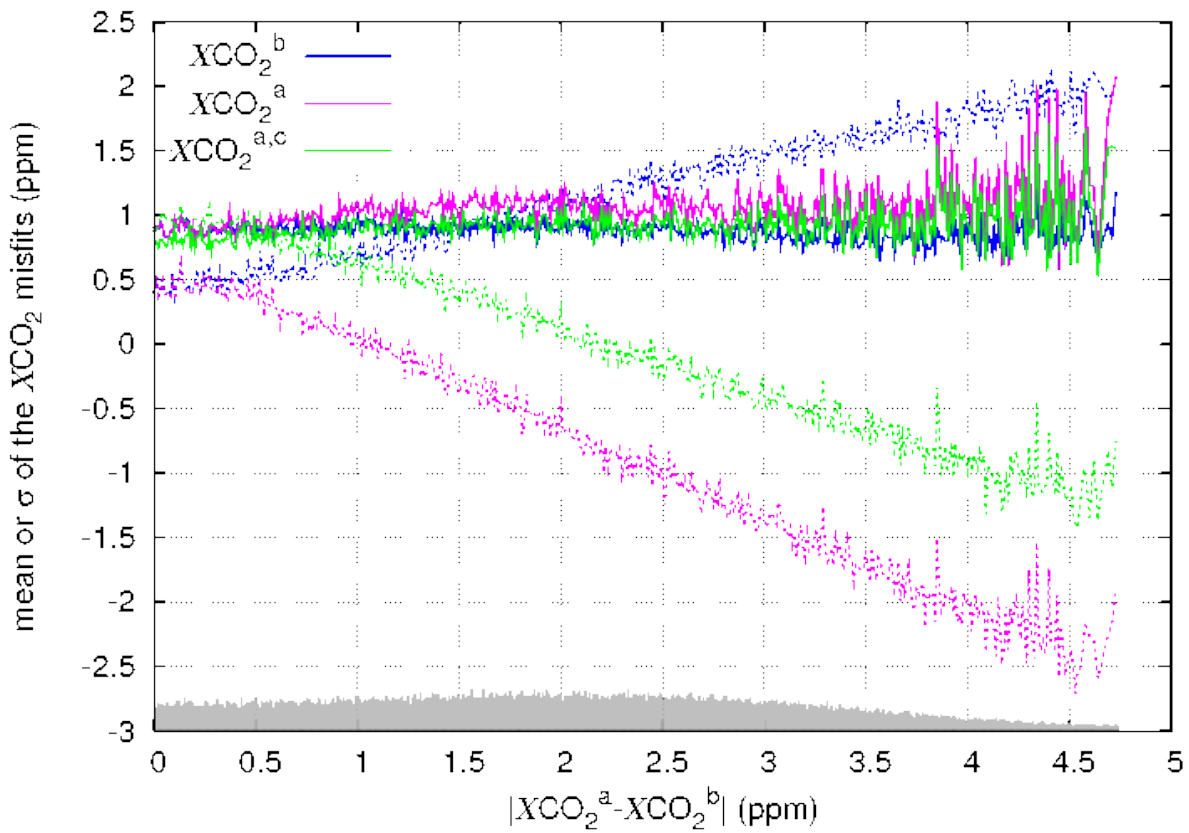


689

690 **Fig. 6. Same as Fig. 5 (high-gain mode over the lands) but we reduce the retrieval increment**  
 691 **size by 50% without any bias correction (we call  $XCO_2^{a,r}$  the result). The abscissa shows the**  
 692 **unperturbed increment.**

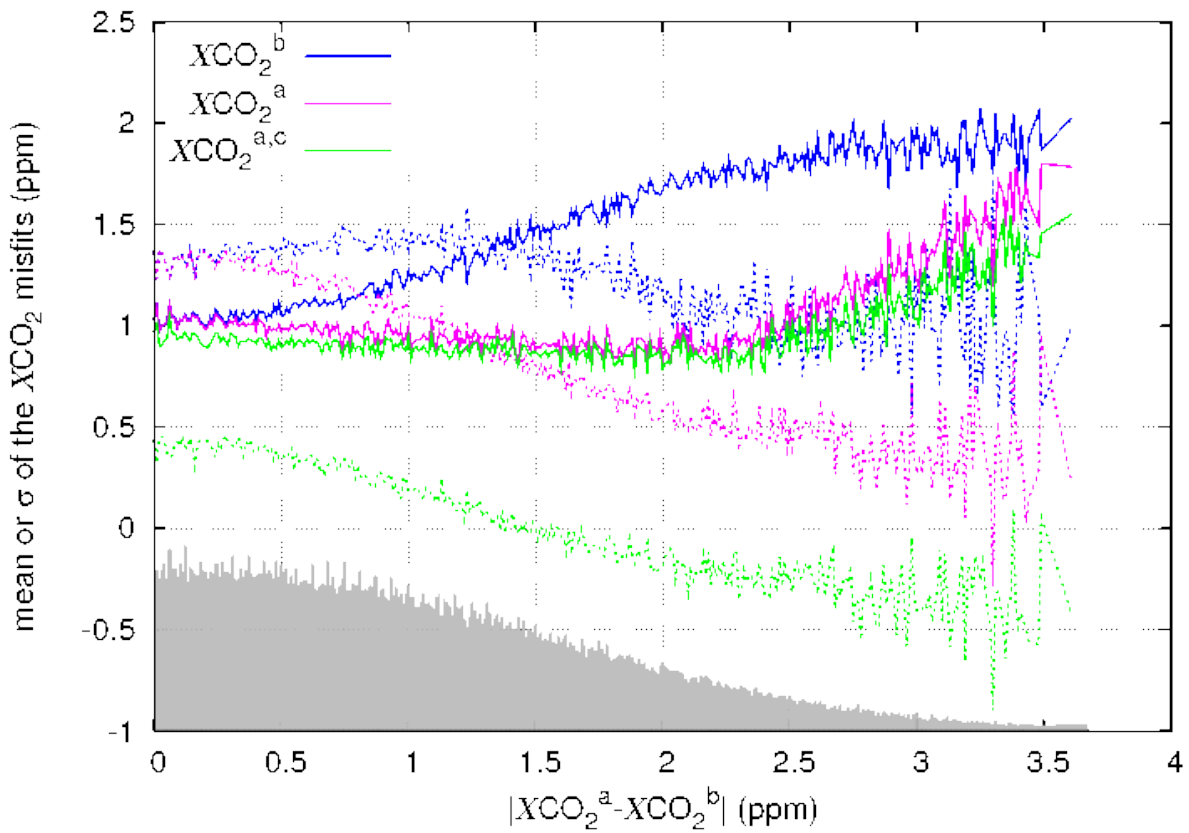
693

694



695

696 **Fig. 7. Same as Fig. 5 for the medium-gain mode.**



697

698 **Fig. 8. Same as Fig. 5 for the glint mode over the ocean.**

699